Heliyon 10 (2024) e30433

Contents lists available at ScienceDirect

Heliyon

journal homepage: www.cell.com/heliyon

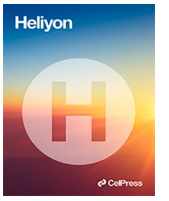

Research article

The application of proteomics and phosphoproteomics to reveal the molecular mechanism of salidroside in ameliorating myocardial hypoxia

Zhongwei Xu [a,1], Kaiyuan Fan [a,b,1], Heng Li [a,c,1], Lulu Wang [d,1], Wenqing Zhu [a], Shuang Zou [a], Yan Zhang [a], Yanan Liu [a], Zhidong Wu [a], Qian Gong [c], Minjia Tan [d], Jin Wang [c,*], Linhui Zhai [b,d,e,**]

[a] *Central Laboratory, Logistics University of Chinese People's Armed Police Force, Tianjin, 300309, China*
[b] *Translational Research Institute of Brain and Brain-Like Intelligence, Shanghai Fourth People's Hospital, School of Medicine, Tongji University, Shanghai, 200434, China*
[c] *Department of Clinical Laboratory, Tianjin Third Central Hospital, Tianjin, 300170, China*
[d] *State Key Laboratory of Pharmaceutical Research, Shanghai Institute of Materia Medica, CAS, Shanghai, 201203, China*
[e] *Jiangsu Key Laboratory of Marine Pharmaceutical Compound Screening, College of Pharmacy, Jiangsu Ocean University, Lianyungang, 222005, China*

ARTICLE INFO

Keywords:
Salidroside
Myocardial hypoxia
Proteome
Phosphoproteome
Aurora kinase

ABSTRACT

Salidroside (SAL), belonging to a kind of the main active ingredient of *Rhodiola rosea*, is extensively utilized for anti-hypoxia and prevention of altitude sickness in the plateau region of China. However, the research on the systemic changes induced by SAL at intracellular protein level is still limited, especially at protein phosphorylation level. These limitations hinder a comprehensive understanding of the regulatory mechanisms of SAL. This study aimed to investigate the potential molecular mechanism of SAL in ameliorating the acute myocardial hypoxia induced by cobalt chloride using integrated proteomics and phosphoproteomics. We successfully identified 165 differentially expressed proteins and 266 differentially expressed phosphosites in H9c2 cells following SAL treatment under hypoxic conditions. Bioinformatics analysis and biological experiment validation revealed that SAL significantly antagonized $CoCl_2$-mediated cell cycle arrest by downregulating CCND1 expression and upregulating AURKA, AURKAB, CCND3 and PLK1 expression. Additionally, SAL can stabilize the cytoskeleton through upregulating the Kinesin Family (KIF) members expression. Our study systematically revealed that SAL had the ability to protect myocardial cells against $CoCl_2$-induced hypoxia through multiple biological pathways, including enhancing the spindle stability, maintaining the cell cycle, relieving DNA damage, and antagonizing cell apoptosis. This study supplies a comprehension perspective on the alterations at protein and protein phosphorylation levels induced by SAL treatment, thereby expanded our knowledge of the anti-hypoxic mechanisms of SAL. Moreover, this study provides a valuable resource for further investigating the effects of SAL.

* Corresponding author. Department of Clinical Laboratory, Tianjin Third Central Hospital, Tianjin, 300170, China.
** Corresponding author. State Key Laboratory of Pharmaceutical Research, Shanghai Institute of Materia Medica, CAS, Shanghai, 201203, China.
E-mail addresses: wangjane0917@126.com (J. Wang), zhailinhui@simm.ac.cn (L. Zhai).
[1] These authors contributed equally: Zhongwei Xu, Kaiyuan Fan, Heng Li, and Lulu Wang.

https://doi.org/10.1016/j.heliyon.2024.e30433
Received 10 January 2024; Received in revised form 14 March 2024; Accepted 25 April 2024
Available online 28 April 2024

1. Introduction

Maintaining a sufficient supply of oxygen is crucial for sustaining the heart myocardium's energy levels and structural stability [1]. Hypoxia, characterized by low oxygen levels, is prevalent in various environments such as high altitudes, tunnels, underwater environments, and plateaus [2,3]. Individuals with cardiovascular and cerebrovascular diseases are also at risk of experiencing hypoxia. Research has demonstrated that consistent and stable exposure to hypoxia can induce a compensatory stress response in the body that facilitates adaptation to low oxygen levels [4]. This adaptive mechanism is advantageous for maintaining homeostasis and internal environment stability. However, prolonged or excessive exposure to hypoxic stress can be detrimental if the body fails to sustain its compensatory response. This can lead to inadequate energy supply in vital organs like the heart and brain ultimately resulting in mortality [5].

Abbreviation

SAL	salidroside
ROS	reactive oxygen species
SOD	superoxide dismutase
SILAC	stable isotope labeling with amino acids in cell culture
$CoCl_2$	Cobalt chloride
AGC	auto-gain control
HCD	higher-energy collision energy dissociation
NCE	normalized collision energy
LP	localization probability
$\triangle\Psi$ m	mitochondrial membrane potential
VR	viability rate
NO	nitric oxide
DEP	differently expressed protein
DPS	different phosphosite
BP	biological processes
PPI	Protein-Protein Interaction (PPI)
HIF1A	hypoxia-inducible factor 1 alpha subunit
HMOX1	heme oxygenase
SRXN1	sulfiredoxin 1
KEAP1	KELCH like ECH associated protein 1
ROMO1	reactive oxygen species modulator 1
CHAF	chromatin assembly factor 1A
MKI67	marker of proliferation Ki-67
PLK1	polo-like kinase 1
TIMELESS	timeless circadian regulator
CDCA5	cell division cycle associated 5

Residents living in high-altitude areas in south Sichuan and Tibet, China often turn to traditional Chinese medicines such as *Ginseng, Codonopsis pilosula, Rhodiola rosea,* and *Pollen* to enhance their physiological adaptability and prevent altitude sickness [6–9]. *Rhodiola rosea* is extensively utilized in China due to its anti-aging, anti-inflammatory, anti-tumor, and hypoxia-antagonizing effects [10]. Salidroside (SAL), an active component found in *Rhodiola rosea* has been shown to have protective effects against cell death caused by various stresses [11]. Studies have revealed that SAL can promote angiogenesis and reconstruction by upregulating the expression of vascular endothelial growth factor and kinase inserts domain receptor [12,13]. SAL has also been reported to have the ability to delay cardiac aging and endocrine function decline, reduce ventricular tachycardia and ventricular fibrillation caused by ischemic myocardial reperfusion. SAL also exhibits anti-arrhythmic effects [14]. Additionally, SAL can remove excessive reactive oxygen species (ROS) and inhibit lipid peroxidation through increasing the production of superoxide dismutase (SOD) and glutathione peroxidase [15–18]. Furthermore, SAL has proven effective in improving the cardiac function of patients with ischemia-reperfusion injury, reducing myocardial cell injury after reperfusion, and decreasing inflammation by lowering creatine kinase, lactate dehydrogenase, tumor necrosis factor α, interleukin-1β, and interleukin-6 [19].

Despite numerous previous studies investigating the potential mechanisms underlying SAL's anti-hypoxic effects, most have focused on individual proteins or pathways, lacking a comprehensive understanding of the dynamic changes occurring in intracellular proteins following drug administration. Limited proteomic studies have been conducted on salidroside, providing partial insights into protein-level changes; however, these investigations were confined to alterations in protein expression levels. Post-translational modifications (PTMs), particularly phosphorylation modifications, play an indispensable role in cellular signal transduction and are pivotal for elucidating the mechanisms of drug action. Previous investigations on SAL have not explored alterations in the post-translational modification level, thus impeding a comprehensive understanding of the regulatory mechanisms underlying SAL.

Proteomics and phosphoproteomics technologies are widely used in the field of life sciences due to they provide systematic approaches for global quantifying proteins, phosphoproteins, and phosphorylation sites within cells under diverse conditions [20]. The present study applied an integrated proteomics strategy to elucidate SAL's comprehensive mechanism against myocardial hypoxia. This study supplies a comprehension perspective on the alterations at protein and protein phosphorylation levels induced by SAL treatment, thereby expanded our knowledge of the anti-hypoxic mechanisms of SAL.

2. Experimental section

2.1. Chemicals and reagents

Salidroside (SAL) (purity >99 %) was from the National Institute for Food and Drug Control (Beijing, China). Cobalt chloride ($CoCl_2$) was from Sigma Aldrich (St. Louis, MO). Custom-synthesized cell culture medium(A33822) without arginine, lysine, methionine, and dialyzed fetal bovine serum (30067334) was from Gibco (NY, USA). L-arginine-$^{13}C_6^{15}N_4$ hydrochloride (PR-25509) (99 % purity), L-arginine-$^{13}C_6$ hydrochloride (PR-24596) (99 % purity), L-lysine-$^{13}C_6^{15}N_2$ hydrochloride (PR-24135) (99 % purity) and L-lysine-4,4,5,5-D4 hydrochloride (PR-25270A) (96–98 % purity) were from Cambridge Isotope Laboratories. L-Arginine monohydrochloride(A6969), L-Lysine (L9037), and L-Methionine(M5308) were from Sigma-Aldrich. Rabbit monoclonal anti-AURKA (52973), anti-mTOR (134903), anti-CDK6 (124821), anti-HMOX1(68477), anti-KEAP1(119403), anti-SOD2(68155), anti-MAPK1 (32537), anti-MAP4K4(155583) antibodies were from Abcam. HRP labeling anti-rabbit IgG, anti-mouse IgG, and FITC-linked secondary antibodies were from KPL (Gaithersburg, MD). Mitochondrial membrane potential JC-1, CCK-8, and cell cycle kits were from the YEASEN company (Shanghai, China).

2.2. Cells culture

The rat cardiomyoblast cell line H9c2 (catalog: CL-0089) were kindly provided by Pricella Life Science&Technology Co.,Ltd, and free of mycoplasma contamination. Cells were cultivated in Dulbecco's modified Eagle's medium (DMEM), which contained 10 % dialyzed fetal bovine serum (FBS), at a temperature of 37 °C while exposed to a 5 % CO_2 atmosphere. In order to perform stable isotope labeling with amino acids in cell culture (SILAC) labeling, cells were grown as usual, but with the inclusion of $^{12}C_6$-Lysine (Lys0) and $^{12}C_6$-Arginine (Arg0) to create the light condition; and 4,4,5,5-D_4-Lysine (Lys4) and $^{13}C_6$-Arginine (Arg6) for the medium state. The heavy condition was achieved by introducing $^{13}C_6$,$^{15}N_2$-Lysine (Lys8) and $^{13}C_6$,$^{15}N_4$-Arginine (Arg10). During triple-labeled experiments, lysine and arginine concentrations were consistently set at 0.798 and 0.398 mmol/L. To ensure protein quantification accuracy, a concentration of 200 mg/L proline was added to the culture medium to prevent the arginine-to-proline conversion process. The H9c2 cells were cultured in triple-labeled culture media and passaged every 3–4 days for a total of 24 days to achieve complete SILAC incorporation.

2.3. CCK-8 assay

The cells were subjected to mycoplasma testing and found to be free of contamination. A total of 1×10^4 H9c2 cells were cultured in 96-well plate containing sophisticated media with 10 % FBS for 12 h. Cells were pre-treated with 1 μmol/L SAL for 24 h and treated with 500 μmol/L cobalt chloride for 1, 3, 6, and 12 h. CCK-8 assay was performed as described previously [21]. The optical density (OD) value was measured at 570 nm using the SpectraMax Series Microplate Reader (Sunnyvale, CA, USA). Each sample was assayed in triplicate.

2.4. Assessment of oxidative stress level of H9c2 cells

Cells were seeded into a 75 cm^2 flask at a concentration of 1×10^6 followed by treated as previously described [22]. The intercellular oxidative damage levels were measured using the SOD Assay Kit (S0101), ROS Assay Kit (S0033), and DAF-FM DA (S0019). Cells were lysed with lysis buffer on ice for 5 min, and the supernatant was collected after centrifuging at 12000 rpm for 5 min. SOD in the supernatant was detected using WST-8 working solution. The OD value was detected using SpectraMax Series Microplate Reader (Sunnyvale, CA, USA). According to the protocol, cells in each group were digested with 0.25 % trypsin, followed by incubation with 5 μmol/L DAF-FM DA or 10 μmol/L DCFH-DA. The excitation wavelength for ROS detection was 488 nm, the absorption wavelength was 525 nm, the excitation wavelength for DAF-FM DA detection was 495 nm, and the absorption wavelength was 515 nm. The value of SOD was measured at 450 nm. The inhibition rate of SOD was calculated using the following formula: Inhibition rate=$((OD_{Control}-OD_{Blank})-(OD_{Sample}-OD_{Blank}))/(OD_{Control}-OD_{Blank}) \times 100$ %.

2.5. SILAC and sample preparation for proteomics and phosphoproteomics analysis

SILAC-based quantitative proteomics and phosphoproteomics analysis were performed to investigate the potential changes in the H9c2 cell proteome in response to the SAL-mediated anti-hypoxia effects. As the control group, H9c2 cells were cultured under the light-labeled condition, and cells were treated with 500 μmol/L cobalt chloride for 12 h under the medium-labeled condition. After being pre-treated with 1 μmol/L SAL for 24 h, cells were treated with 500 μmol/L cobalt chloride for 12 h under the heavy labeled condition. The cells were washed four times with ice-cold phosphate-buffered saline (PBS) and suspended in cell lysis buffer (8 M Urea,

30 mM NaCl, 5 mM Na_4PO_7, 100 mM NaH_2PO_4 (pH = 8.0), 1 mM NaF, 1 mM Na_3VO_4, 1 mM sodium glycerophosphate, protease inhibitor cocktail (Thermo, A32963), phosphatase inhibitor cocktail (Thermo, 78420)). The solution was then ultrasonicated at 25 % maximum power (JY92-IIN) for 10 min on ice and centrifuged at 4 °C with 13,000 g for 10 min. The supernatant was collected and the protein concentration in each group was detected by using Bicinchoninic Acid Assay (BCA) (Pierce, Thermo Fisher Scientifc, Inc.).

Equal amounts of protein from each light (1 mg), medium (1 mg), and heavy-labeled samples (1 mg) were mixed, and 3 mg protein mixtures of triple labeled experiments were reduced with 10 mmol/L DTT and alkylated with 50 mmol/L IAA and followed by in-solution digested with 12.5 ng/μL of trypsin at 37 °C for 16 h, as described previously [23]. After digestion overnight, peptides were desalted with Sep-Pak tC_{18} 1 cc Vac Cartridge (WAT054960, Waters), dried with vacuum centrifugation, and stored at −80 °C.

1 mg combined peptides were separated using offline high-pH reverse-phase chromatography. In brief, the dried peptides were resuspended in high-pH mobile-phase A (2 % acetonitrile (ACN) and 98 % H_2O (adjusted to pH = 9.0 with ammonia water)) and then loaded onto Xbridge® Peptide BEH C_{18} column (3.5 μm, 4.6 × 250 mm, Waters, Milford, MA) equipped on an Agilent 1100 HPLC system. The peptides were eluted with a 60-min gradient of 3 %–80 % high-pH mobile-phase B (98 % ACN and 2 % H_2O (adjusted to pH = 9.0 with ammonia water)) at a 0.6 mL/min flow rate. Fractions were collected each minute and finally combined into 15 fractions. All the fraction samples were dried with vacuum centrifugation and stored at −80 °C before nano-LC-MS/MS analysis.

According to the previous description [24], the phosphopeptides of the rest of the 2 mg combined peptides were enriched by TiO_2 affinity chromatography using magnetic microspheres (PT0850, GL Sciences Inc.) and a magnetic separator (Thermo Fisher Scientific). Briefly, an amount of ~4 mg TiO_2 magnetic microspheres was washed three times with 70 % (v/v) ethanol and equilibrated once in 1 % NH_4OH and four times in phosphopeptides loading buffer (1 mol/L glycolic acid in 80 % (v/v) acetonitrile (ACN), 5 % (v/v) trifluoroacetic acid (TFA)). ~2 mg of tryptic peptides were diluted in 1 mL loading buffer (50 % (v/v) ACN, 0.25 % TFA, 80 mmol/L lactic acids), added to 4 mg of equilibrated magnetic microspheres, and incubated for 20 min at RT with continuous rotation. After binding of the phosphopeptides, the microspheres were washed once with loading buffer, and three washes removed unbound peptides with washing buffer (80 % (v/v) ACN, 1 % (v/v) TFA). Phosphopeptides were performed a six-time gradient elution by buffer containing 15 % (v/v) NH_4OH and 0, 2, 5, 8, 10, 40 % (v/v) ACN. The phosphopeptides in each gradient elution were desalted using C_{18} ZipTips (Millipore). Peptides were resuspended in 3 % (v/v) ACN, 0.1 % (v/v) TFA, and desalted using C_{18} ZipTips (Millipore) and followed by dried in a SpeedVac concentrator. The peptides and phosphopeptides of each fraction were dissolved in 10 μl of solvent (3 % (v/v) ACN, 0.1 % (v/v) FA) before LC-MS/MS analysis.

2.6. nanoLC-MS/MS detection and data analysis

The peptides were analyzed by a nano-liquid chromatography system (EASY-nanoLC 1000, Thermo Fisher) connected with an Orbitrap Fusion mass spectrometer (Thermo Fisher) [25]. For the quantitative proteome sample, the fractioned peptides were resolved in buffer A (0.1 % formic acid (FA), 2 % ACN in H_2O) and directly loaded onto a home-made reverse-phase capillary analytical column (75 μm ID × 20 cm length) packed with C_{18} resin (1.9 μm particle size, 100 Å pore size, Dr. Maisch). The peptides were separated by a 60-min gradient of 5 %–40 % buffer B (0.1 % FA in 90 % ACN in H_2O) for 50 min and 40−80 % buffer B for 5 min at a constant flow rate of 300 nL/min on EASY-nLC 1000 system. The eluted peptides were ionized under 2.2 kV high voltage and analyzed by the mass spectrometer. The scan range for a total mass scan was 350–1300 *m/z*. Orbitrap detected the ions with a resolution of 120,000 (*m/z* 200). The auto-gain control (AGC) was established at 1×10^6. For MS/MS scan, the ions with intensity above 5000 were isolated and fragmented by Higher-energy collisional dissociation (HCD) with normalized collision energy (NCE) set at 32 %. The fragment ions were detected in the ion trap, and the AGC was set at 7000. The MS/MS acquisition was performed in full-speed mode with a cycle time was 3 s. The dynamic exclusion duration was set as 60 s. For the phosphoproteome samples, the peptides were separated by a 90-min gradient at a flow rate of 350 nL/min (0–70 min, 4–30 % buffer B; 70–80 min, 32%–40 % buffer B; 80–85 min, 40%–80 % buffer B; and 85–90 min, 80 % buffer B). Orbitrap Fusion also detected the eluted peptides under OT (Orbitrap)-IT (ion trap) mode. In brief, for a total mass scan, the scan range was 350–1400 *m/z*, the resolution was 120,000 (*m/z* 200), and the AGC target was set to 5×10^5. For MS/MS scan, the ions were fragmented by HCD mode with 32 % NCE. The cycle time was 3 s, and the AGC was 7000. The dynamic exclusion duration was 60 s, and the maximum injection time was 40 s.

The MS/MS raw data were searched by the MaxQuant (version 1.5.3.8) search engine against proteome database and the target-decoy strategy was used to control the identification FDR. The target proteins were derived from the UniProt *Rattus norvegicus* database (release 2022_08), and the decoy proteins were produced from pseudo-reversed sequences of the target proteins. Search parameters: precursor ions were searched with an initial mass tolerance of 10 ppm. The False discovery rate (FDR) of peptides and proteins less than 1 % was accepted based on the number of accepted decoy hits. Only *b* and *y* ions were considered during the database search. Enzyme specificity was trypsin/P with two missed cleavages and peptides with at least 7 amino acids. The cysteine carbamidomethylation and methionine oxidation were selected as static modifications. MaxQuant was used to determine the SILAC state of peptides by the mass differences between SILAC peptide pairs. This information was used to perform searches with fixed Arg0 and Lys0, Arg6, and Lys4 or Arg10 and Lys8 modifications appropriate for quantitative proteomics analysis. Otherwise, "Phospho STY" was added as a variable modification for phosphoproteomics analysis. Quality control indexes of phosphoproteomics were applied as described [26]. Briefly, only spectral matches with a delta score of >8 and a PEP score of <0.01 were allowed, and phosphosites with a localization probability (LP) of >0.75 were adopted.

2.7. Bioinformatics analysis

Gene Ontology (GO) information for differentially expressed proteins and phosphoproteins was submitted to DAVID (version 6.8)

for analysis, and the background and species were set to the *R. norvegicus* [27]. The enriched signaling pathways and protein-protein interaction(PPI) were generated using Metascape and Cytoscape (version 3.7.0), and the cluster analysis of differential protein cluster analysis was used Heatma [28].

2.8. Cell apoptosis and cells cycle

Flow cytometry measured the apoptosis and necrosis of cells using AnnexinV/PI labeling. Annexin V/PI Detection Kit (BD Pharmingen, CA) was used to perform according to the instructions. A total of 2×10^5 H9c2 cells were cultured in a 10 cm diameter dish for 12 h. After cells were treated with or without 1 μmol/L SAL for 24 h, cells were treated with 500 μmol/L cobalt chloride for 12 h, followed by trypsinized and fixed in a mixture of 70 % ethanol and 30 % PBS. Cells were incubated with buffer (25 μg/mL PI, 40 μg/mL RNase A) at room temperature for 45 min. The cell apoptosis cell cycle was analyzed using FlowJo (version 10.4).

2.9. Mitochondrial membrane potential ($\triangle\Psi m$)

A total of 2×10^3 H9c2 cells were cultured in a 2 cm confocal dish for 12 h. After cells were treated according to the previous description, cells were incubated with 1 mL JC-1 staining buffer for 20 min at 37 °C. Cells were visualized using a confocal microscope (objective: 40, Leica TSP SP8, German). The Max absorption/emission wavelength for green and red fluorescence was 510/527 nm and 585/590 nm, and fluorescence intensity was analyzed using Image Pro Plus software (version 10.4).

2.10. Mn^{2+}-phos-tag SDS-PAGE gels and Western blot

Lysates of H9c2 cells after hypoxia and anti-hypoxia treatments were prepared using a nondenaturing lysis buffer (50 mmol/L Tris–HCl (pH 7.4), 0.15 mmol/L NaCl, 0.25 % (w/v) sodium deoxycholate, 1.0 % (v/v) NP-40, protease inhibitor cocktail (Thermo, A32963), phosphatase inhibitor cocktail (78420)), as previously described [29]. Gels were prepared according to the manufacturer's protocol (APExBIO) using Phosbind (No. F4002). The rabbit anti-HIF1A (1:2000), HMOX1(1:3000), Keap1(1:1000) and anti-mTOR (1:2000) antibodies were applied to the Western blot according to the previous description. The Mn^{2+}-phos-tag gels and Western blot were implemented [30]. Briefly, approximately 60 μg of protein samples were operated on the 4–12 % of Mn^{2+}-Phos-tag SDS-PAGE gels and run for 4 h at 60 V and then transferred to nitrocellulose membranes (Amersham) followed by blocked and incubated using primary antibodies: The rabbit anti- MAPK1(1:1000), MAP4K4 (1:1000), AURKA (1:2000) and CDK6 (1:1000). After

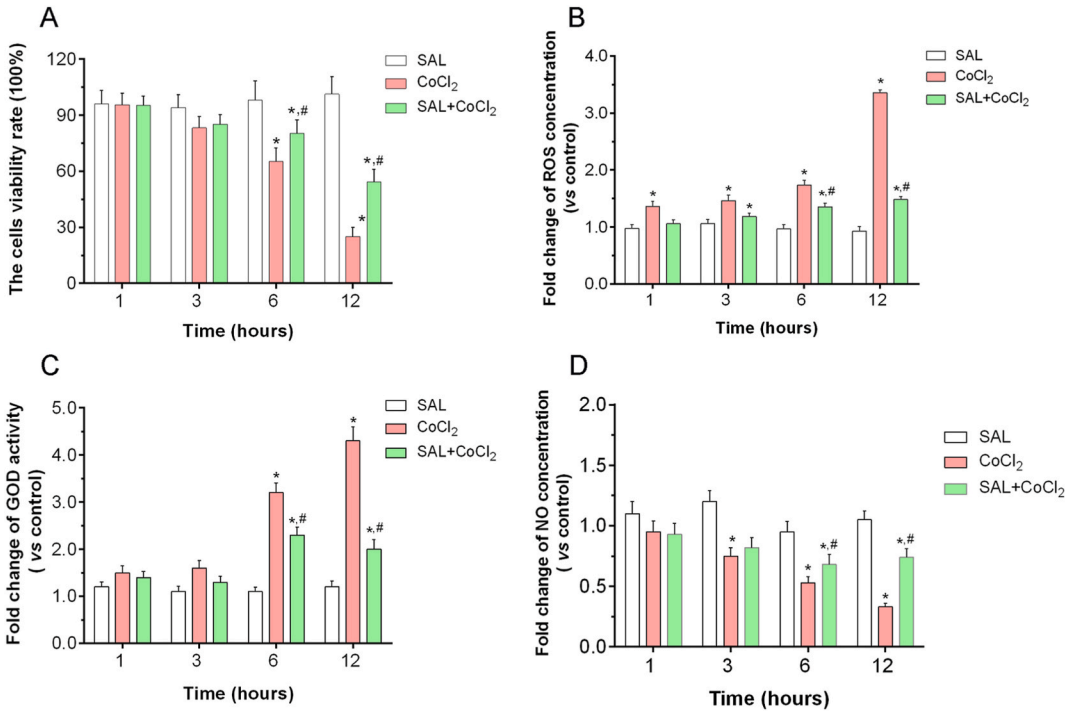

Fig. 1. Effects of SAL in the viability and oxidative damage of H9c2 cells treated by $CoCl_2$. (A) The cell viability rate comparison among treated with DMSO, 500 μmol/L $CoCl_2$ and SAL combo with 500 μmol/L $CoCl_2$. (B–D) Effects of SAL on the intracellular ROS, GOD and NO of H9c2 cells (n = 3 per group). Data are represented as mean ± standard deviation according to one-way ANOVA, compared to control group, $^*p < 0.05$; compared to $CoCl_2$ treatment group, $^{\#}p < 0.05$.

washing three times, membranes were incubated with a secondary antibody (1:10000). The blots were visualized with ECL reagents (KPL, U.S.A), followed by capture with the Amersham Imager 600 system (GE, UK). The intensity of blots was performed using ImageQuant TL (GE, UK).

2.11. Statistical analysis

The data were presented as mean ± SD and analyzed using SPSS (version 26.0). ONE-WAY ANOVA was applied to identify different groups. $P < 0.05$ was considered as statistically significant.

2.12. Data availability

All the mass spectrometry proteomics raw data and the database search result data have been deposited to the iProX with the dataset identifier IPX0006851000.

3. Results

3.1. Effects of SAL on cell proliferation and oxidative damage under $CoCl_2$-induced hypoxia condition in H9c2 cells

As shown in Fig. 1A, the viability rate (VR) of H9c2 cells was not significantly changed between the control and SAL groups ($P > 0.05$). The VR of $CoCl_2$ treatment for 6 h and 12 h was significantly decreased compared with control groups ($^*P < 0.05$). However, under cobalt chloride treatment for 6 h and 12 h, the VR was significantly increased in H9c2 cells pretreated with 1 μmol/L SAL for 24 h ($^{\#}P < 0.05$). Compared with the control group, the concentration of intracellular ROS and activity of SOD in $CoCl_2$ treatments at different time spots was significantly increased ($^*P < 0.05$), and those in SAL treatment groups were significantly decreased compared with their respective $CoCl_2$ treatment ($^{\#}P < 0.05$). Meanwhile, the levels of nitric oxide (NO) were obviously decreased in cells treated with $CoCl_2$ for 6 and 12 h compared with the control group ($^*P < 0.05$), and SAL could attenuate the trend induction by $CoCl_2$ ($^{\#}P < 0.05$). Such phenotypic evidence suggested that SAL could antagonize the hypoxia effects induced by $CoCl_2$ in H9c2 cells.

The quantitative proteome and phosphoproteome analysis constructed an expression landscape of the proteins and phosphoproteis

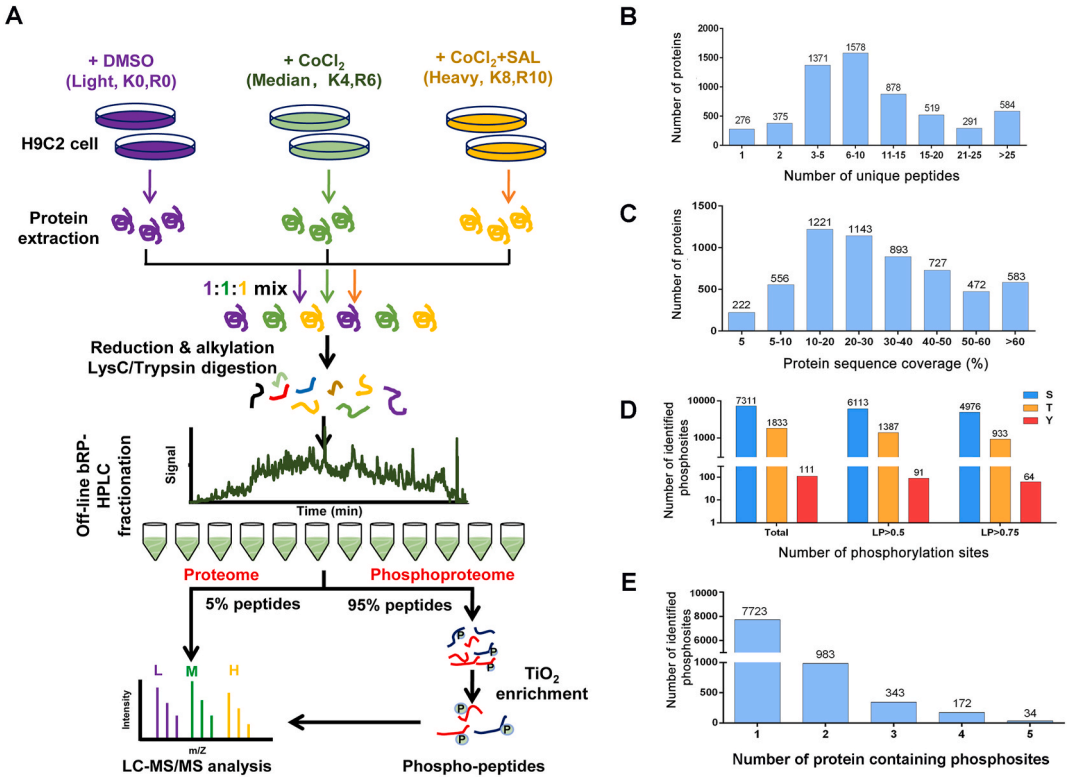

Fig. 2. Quantitative proteomics and phosphorylation proteomics of H9c2 cells under $CoCl_2$-induced hypoxia and SAL-mediated anti-hypoxia conditions based on the SILAC strategy. (A) Technique flowchart of integrated proteomics. (B) Map of the quantity distribution of unique peptides on proteins. (C) The analysis of identified protein sequence coverage. (D) Quantity and quality control of different phosphorylation sites. (E) Quantity and quality control of different phosphopoteins.

in response to SAL treatment.

To elucidate the molecular mechanism underlying the anti-hypoxic effects of SAL, we performed SILAC-based proteomics and phosphoproteomics analysis in H9c2 cells treated with SAL or $CoCl_2$ (Fig. 2A). In the quantitative proteomics analysis, a total of 5872 proteins were identified and 5321 proteins were quantified. Among all the identified proteins, only 11 % (276 and 375 proteins) had one or two peptides (Fig. 2B). Additionally, only 3.8 % (222 proteins) of the identified proteins had less than 5 % protein sequence coverage (Fig. 2C). These results indicated the high quality of proteomics data in this study. Through phosphoproteomics analysis, we totally identified 9255 phosphorylation sites, including 7311 phospho-S sites, 1833 phospho-T sites, and 111 phospho-Y sites. High confidence phosphorylation sites with localization probability (LP) > 0.5 and LP > 0.75 accounted for 82.0 % and 64.5 % of the total sites, respectively (Fig. 2D). The phosphoproteomics results showed 7723 proteins with one phosphorylation site while 983, 343, 172, and 34 proteins had two, three, four, and five phosphorylation sites, respectively (Fig. 2E). The cutoff criteria to identify the differentially expressed proteins (DEPs) and differentially expressed phosphoproteins were set as a combination of a p-value <0.05 and 1.5-fold change in quantitative proteomics and phosphoproteomics data, respectively. A total of 504 DEPs were identified between the $CoCl_2$ treatment group and control group, with 346 DEPs down-regulated and 158 up-regulated (Supplementary Table S1). Gene Ontology (GO) analysis significantly enriched these DEPs into several vital biological processes (BPs), including cell cycle regulation, chromosome organization, Rho GTPase signaling pathway, DNA metabolism, and ECM-receptor interaction (Fig. S1A). Between the SAL treatment group and the $CoCl_2$ group, a total of 165 DEPs were identified with 52 down-regulated and 113 up-regulated (Supplementary Table S2). These DEPs were significantly enriched into many BPs, including cell cycle regulation, DNA metabolism, DNA replication, chromatin organization, and response to ROS (Fig. S1B). Furthermore, a total of 346 DEPs were identified between the SAL treatment group and the control, with 238 down-regulated and 108 up-regulated (Supplementary Table S3). These DEPs exhibited significant enrichment in supramolecular fiber organization, ECM interaction, response to wounding, and oxidative stress response (Fig. S1C).

The phosphoproteome analysis revealed the identification of 151 different phosphosites (DPSs) between $CoCl_2$ treatment and control groups (Supplementary Table S4). Among these, 12 sites were down-regulated and 139 sites were up-regulated. The proteins associated with these DPSs exhibited significant enriched in various biological processes, including supramolecular fiber organization, protein depolymerization, actin cytoskeleton organization, and signaling by Rho GTPases (Fig. S2A). 266 DPSs in the SAL treatment group were found compared with the $CoCl_2$ treatment group (Supplementary Table S5), with 232 down-regulated and 34 up-regulated. These DPSs were significantly enriched in actin filament-based processes, signaling by Rho GTPases, response to epidermal growth factor, and apoptotic execution phase (Fig. S2B). Compared to control cells, the SAL treatment cells showed 285 DPSs, with 100 down-

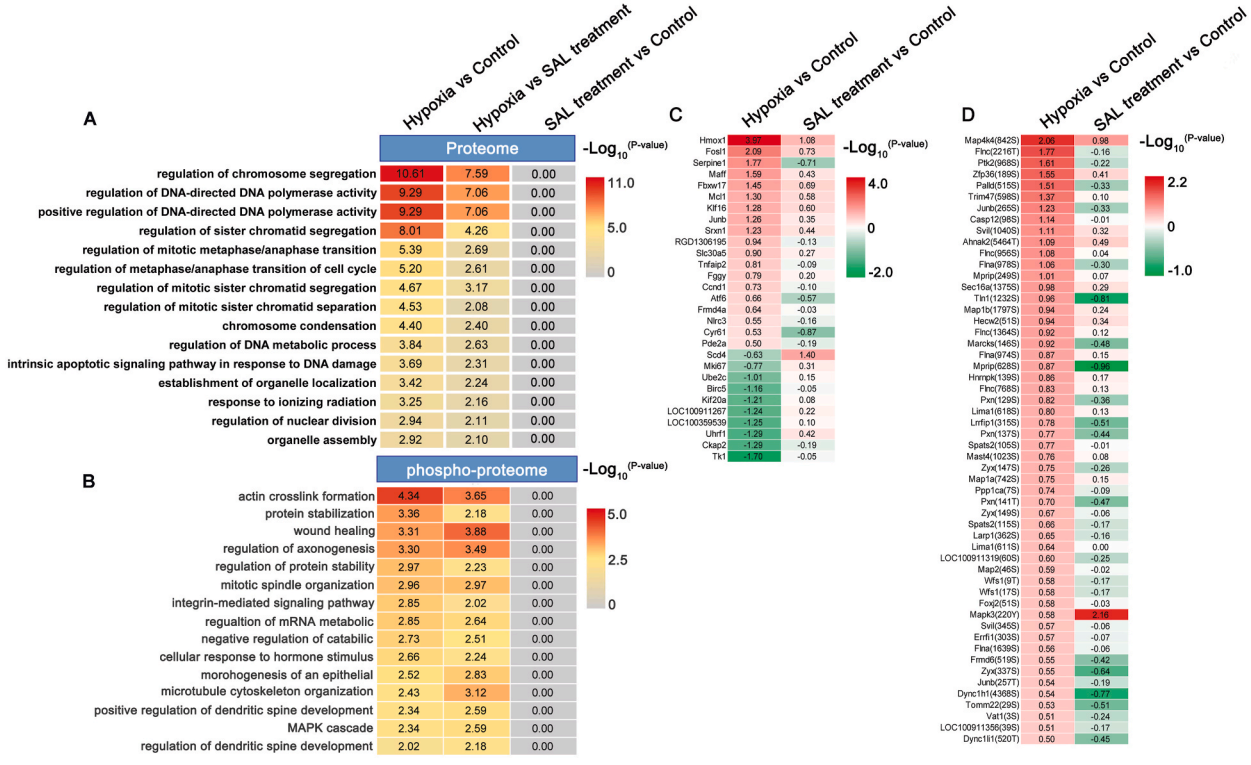

Fig. 3. Heatmap clustering analysis of Top15 biological processes, 29 DEPs and 54 DESs. (A) Heatmap cluster analysis of Top15 BP in quantitative proteomics and quantitative phosphoproteomics. (B–C) Heatmap cluster analysis of differently expressed proteins and phosphoproteins related in anti-hypoxia effects.

regulated and 185 up-regulated (Supplementary Table S6). The corresponding proteins of these DPSs were significantly enriched in actin cytoskeleton organization, establishment of cell polarity, endomembrane system organization, insulin signaling and apoptotic execution phase (Fig. S2C). These phosphoproteomics results suggest that SAL exerts its anti-hypoxic effects through modulating the phosphorylation level in H9c2 cells.

Bioinformatics correlation analysis of proteomics and phosphproteomics for comprehensive understanding.

By comparing GO analysis of quantitative proteomics (Fig. 3A), we found significant enrichment of several important biological processes (BPs) in the $CoCl_2$ treatment group, including chromosome segregation, DNA polymerase activity, cells cycle, and nuclear division ($P < 0.05$). However, these BPs were not significantly enriched in the anti-hypoxia group ($P > 0.05$). Similarly, when comparing the GO analysis of phosphoproteomics (Fig. 3B), we also noticed significant enrichment of crucial BPs such as action crosslink formation, protein stabilization, wound healing, and MAPK signaling, were significantly enriched ($P < 0.05$), which remained unchanged in the anti-hypoxia group. Further analysis of the DEPs involved in these BPs (Fig. 3C and D), 29 proteins (e.g., Hmox1, Fosl1, Serpine1, Fbxw17, Mcl1, Klf16, Tnfaip2, Ccnd1, Atf6, Scd4, Mki67, Kif20a, Ckap2, and Tk1) and 54 phosphoproteins (e.g., Mapk3, Map4k4, Map2, Zyx, Ptk2, Junb Trim47, and Casp12) were obviously different under different conditions. These findings suggest that these proteins play a pivotal role in mediating critical anti-hypoxia effects in H9c2 cells against $CoCl_2$ treatment.

We then restructured the anti-hypoxia signaling network of SAL in response to changing trends by using Cytoscape 3.7 with the plugin Metascape v3.5. The green, blue, and red nodes represented the BPs enriched by DEPs between $CoCl_2$ treatment and control, SAL treatment and $CoCl_2$ treatment group, SAL treatment and control, respectively (Fig. 4). The restructured network revealed that $CoCl_2$-mediated hypoxia and SAL-induced anti-hypoxia effects involved positive regulation of DNA, cell differentiation, extracellular structure, activates PTK2 signaling, cytoskeleton function, response to toxic substance, filament protein depolymerization, and cell cycle processes. Notably, SAL significantly improved cell cycle progression along with DNA replication, cytoskeleton-dependent cytokinesis, and chromosome segregation processes.

3.2. Cells apoptosis, cells cycle and $\Delta\Psi m$

As shown in Fig. 5A, the $CoCl_2$ treatment cells exhibited a significantly increased proportion of early and late apoptosis compared to the control group ($P < 0.05$). Conversely, the SAL treatment cells exhibited obviously decrease in apoptosis proportion when compared

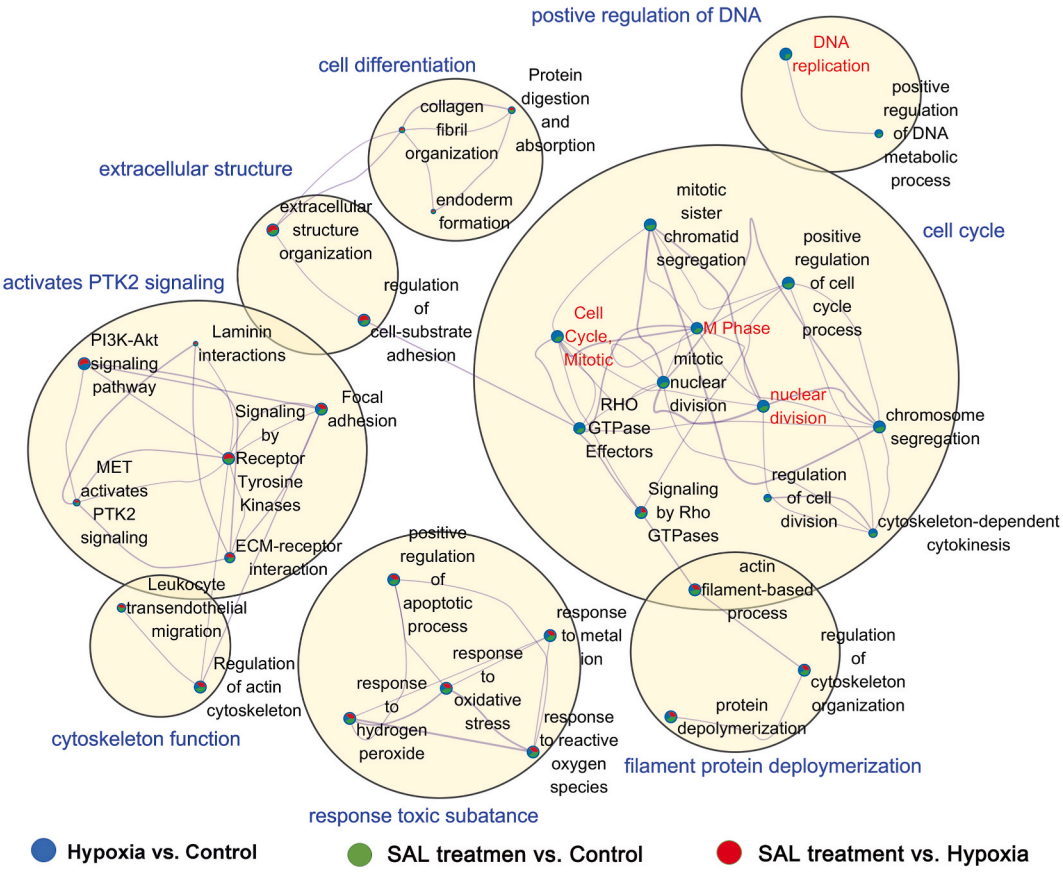

Fig. 4. The anti-hypoxia signaling network of SAL in response to under different treatment. Enrichment analysis of BPs originated from 504, 346 and 165 DEPs in hypoxia vs. control (blue nodes), anti-hypoxia vs. control (green nodes) and anti-hypoxia vs. hypoxia (red nodes), respectively.

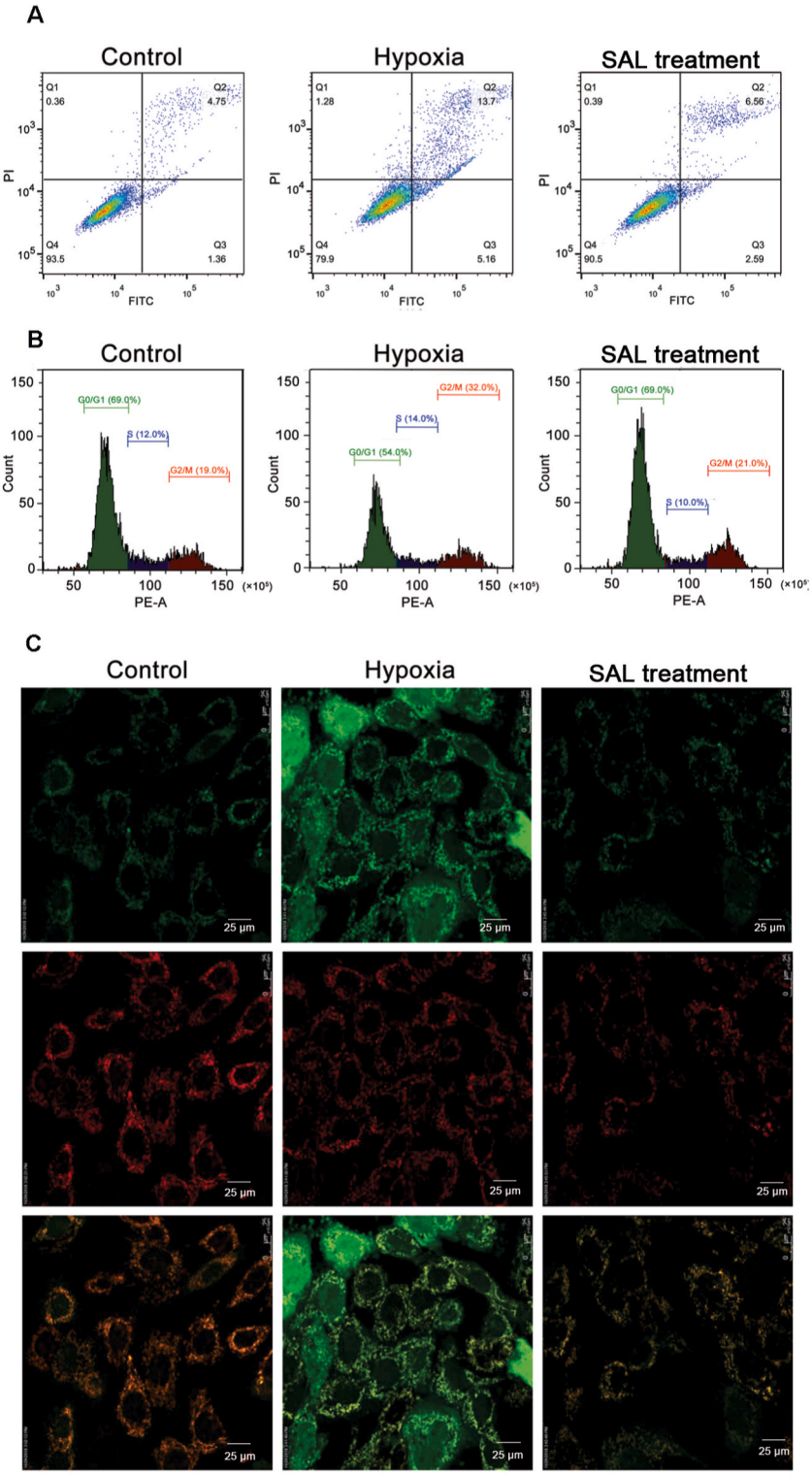

Fig. 5. SAL reduces the $CoCl_2$-induced cells apoptosis, cells cycle arrest and oxidative damage of H9c2 cells. (A) The comparison analysis of apoptotic ratio of cells with under $CoCl_2$ and SAL treatmen. (B) The comparison analysis of distribution of cells cycle using flow cytometry. (C) The comparison of mitochondrial membrane potential analysis. Mitochondrial membrane potential (ΔΨm) was detected by JC-1 staining using confocal microscope (200 ×). Red or green fluorescence represented intact or dissipation of ΔΨm, respectively.

to the cells under $CoCl_2$ treatment ($P < 0.05$). Conversely, the SAL treatment cells demonstrated a noticeable decrease in apoptosis proportion when compared to the cells under $CoCl_2$ treatment ($P < 0.05$). The results from cell cycle analysis revealed a significant reduction in G0/G1 cell proportion in the $CoCl_2$ treatment group (Fig. 5B), accompanied by an evident increase in G2/M cell proportion compared to the control group ($P < 0.05$). Moreover, compared to the $CoCl_2$ treatment group, there was a significant increase in the proportion of cells in G_0/G_1 phase and a marked decrease in those in G_2/M phase. There was no significant difference observed between the SAL treatment and control groups. Additionally, we observed a significant reduction in green fluorescence intensity and ΔΨm with $CoCl_2$ treatment compared to the control group (Fig. 5C). However, the red fluorescence intensity in the SAL pretreatment group was obviously increased and moderated the damage induction by $CoCl_2$. This findings suggest that SAL can play an anti-hypoxia role by altering the cell cycle progression, reducing ROS-induced damage, and suppressing apoptosis in H9c2 cells.

3.3. *Validation of the proteomics and phosphoproteomics results by WB and Mn^{2+}-phos-tag page gels in the H9c2 cell*

The levels of key proteins involved in anti-hypoxia effects were validated by using western-blot technology (Fig. 6). The expression of HIF1A in the anti-hypoxic group pre-treated with SAL for 6h and 12 h were obviously reduced compared to the $CoCl_2$-treated group ($P < 0.05$) (Fig. 6B), while the expression of HMOX1, Keap1, and mTOR in the anti-hypoxic group pre-treated with SAL for 1 h, 3 h, 6 h and 12 h were significantly reduced compared to the $CoCl_2$-induced hypoxia group ($P < 0.05$) (Fig. 6C–E). However, there was no significant difference observed in SOD2 between the SAL-treated anti-hypoxia group and the $CoCl_2$-induced hypoxia group ($P > 0.05$) (Fig. 6F). Even though the expression level of SOD2 protein did not reach statistical significance, significant changes were observed in most key proteins (HIF1A, HMOX1, Keap1, mTOR) involved in anti-hypoxia effects, thereby confirming the anti-hypoxia function of

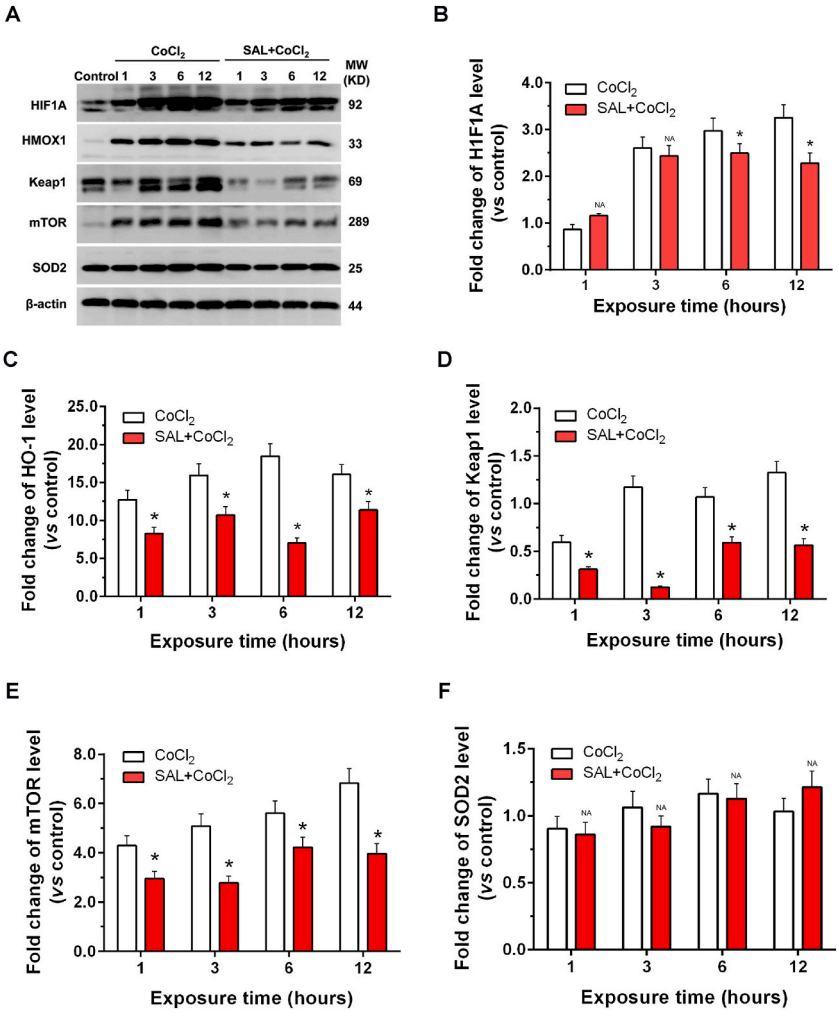

Fig. 6. Validation of critical molecules in quantitative proteomic alterations by Western blot. (A) Western blotting analysis of levels of HIF1A, HMOX1, Keap1, mTOR and SOD. Histograms display the densitometry measurements of bands, with β-actin levels serving as the reference control (n = 3 per group). (B–F) The expression comparison of HIF1A, HO-1, Keap1, mTOR and SOD2 in the anti-hypoxic group pre-treated with combined with SAL $CoCl_2$ and $CoCl_2$-treated group. Data are expressed as the mean ± SD (parametric *t*-test, $^*P < 0.05$).

SAL. We speculate that the lack of statistical significance in SOD2 protein expression levels may be attributed to the minimal difference observed in protein expression between SAL-treatment and $CoCl_2$-treatment, as well as the limited sample size (n = 3 per group) used for verification. The levels of phosphoproteins related to cell cycle, DNA repair, and cytoskeleton function were shown in Fig. 7. The abundance of p-MAP4K4 in the $CoCl_2$-induced hypoxia group for 12 h was significantly increased ($P < 0.05$), whereas the CDK6 expression showed a notable decrease compared to control group ($P < 0.05$) (Fig. 7A). Meanwhile, the *p*-MAKP1, *p*-AURKA and *p*-CDK6 in the anti-hypoxia using SAL treatment were obviously increased compared to those of the $CoCl_2$-induced hypoxia group, and p-MAP4K4 level was significantly decreased ($P < 0.05$) (Fig. 7B–E).

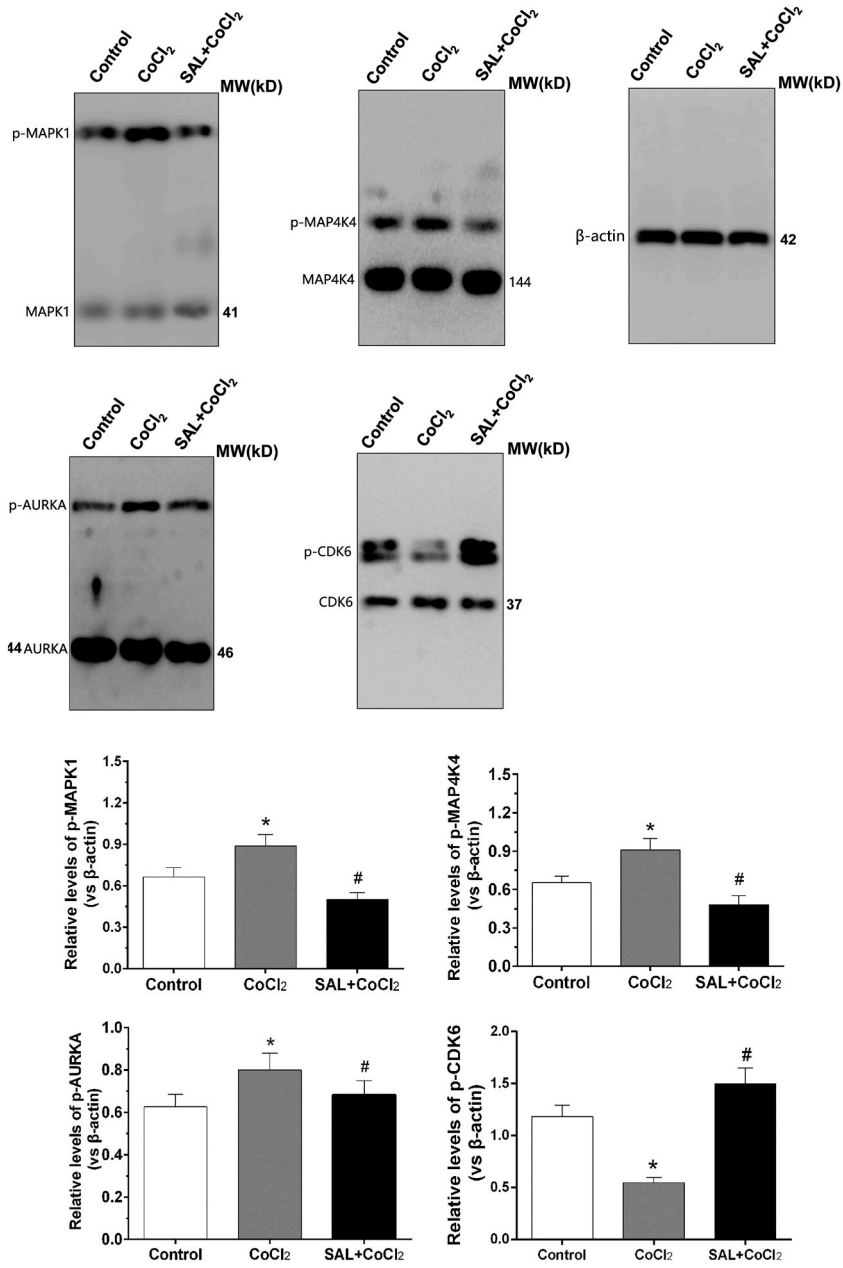

Fig. 7. Validation of critical molecules in quantitative phosphoproteomic alterations by Mn^{2+}-phos-tag SDS-PAGE and Western blot. (A) The phosphorylation level analysis of *p*-MAPK1, p-MAP4K4, *p*-AURKA and *p*-CDK6 by using the phos-tag SDS-PAGE and Western blot analysis. (B–E) The expression comparison of *p*-MAPK1, p-MAP4K4, *p*-AURKA and *p*-CDK6 under different treatment condation. Data are expressed as the mean ± SD (parametric one-way ANOVA, $^*P < 0.05$).

3.4. Mechanism diagram of SAL antagonizing $CoCl_2$-mediated hypoxia

Based on the quantitative proteomics and phosphoproteomics results, we reconstructed the signaling pathway of SAL-mediated anti-hypoxia effects using STRING V11.5. The Protein-Protein Interaction (PPI) network also revealed that 165 DEPs and 266 DPSs were involved in numerous crucial biological processes and signaling pathways (Supplementary Table S7), including cellular response to hypoxia, apoptosis, DNA repair, cell cycle, spindle formation, and focal adhesion (Fig. S3). By analyzing the omics' results, the levels of TP53 and *p*-JUN (70s, 76s) in the SAL treatment group were significantly increased than that of the $CoCl_2$-induced hypoxia group, the levels of HMOX1 and SERPINE1 were obviously decreased. These findings suggest that SAL exerts DNA repair function, pro-proliferation, and anti-senescence function. Moreover, SAL could antagonize $CoCl_2$-induced G_2/M cell cycle arrest by down-regulating CCND1 expression and upregulating AURKA, AURKB, CCND3 and PLK1 expressions. Additionally, SAL can stabilize the cell structures such as spindles and focal adhesions, and inhibit apoptosis through increased the expression of kinesin family (KIF) members, including KIFC1, KIF4A, KIF2C, KIF23, KIF22, KIF20B, KIF20A, and KIF11.

4. Discussion

Rhodiola, a Chinese medicine, also known as "golden root", is widely grown in harsh natural environments characterized by extreme cold, high altitude, and low oxygen levels [31]. There are 96 species of *Rhodiola* in the world, mainly distributed in Asia, Europe and north America. *Rhodiola* has the effect of promoting blood circulation, clearing pulse, and relieving asthma [32]. It is rich in salidroside (SAL), flavonoids, polysaccharides and volatile oil, and other active ingredients. Among these components extracted from the rhizosphere of Rhodiola plants, SAL stands out as the most crucial bioactive compound [33]. Numerous studies have demonstrated that SAL has a unique effect on anti-fatigue, anti-hypoxia, anti-oxidative aging, and the prevention of cardiovascular diseases [34–36]. Hypoxia is a common inducer of many human diseases and despite the complexity of the human system, which is still present throughout the course of many life-threatening diseases [37]. Myocardial hypoxia injury is a common clinical cause of many diseases, such as altitude hypoxia disease, coronary heart disease, hypertensive heart disease, cardiomyopathy, etc [38]. $CoCl_2$ is a widely utilized agent for modeling cellular hypoxia, as it inhibits HIF1A degradation, suppresses the activity of respiratory chain complexes, and induces ROS production [39]. Our study revealed the protective effect of SAL on hypoxia after $CoCl_2$ treatment by promoting cell proliferation, activating AURK signaling, and stabilizing cytoskeletal structure to ameliorate oxidative damage using integrated proteomics and phosphoproteomics strategy.

Previous research on SAL has primarily concentrated on a solitary signaling pathway and has not provided comprehensive clarification, particularly concerning the mechanism of the correlation between SAL's effect on protein phosphorylation and its anti-hypoxic impact. The proteomics and phosphoproteomics provide a comprehensive strategy for quantitatively elucidating biological processes, signaling pathways, and networks in physiological and pathophysiological states at the global protein and protein post-translational modification levels. Compared with the in vitro labeling strategy, the SILAC technique has more accurate quantification, wider linear range, higher sensitivity, and closer to the actual state of cells. Our phenotypic evidence demonstrated that SAL alleviates the hypoxic effects induced by $CoCl_2$ in H9c2 cells.

A total of 165 DEPs and 266 DPSs were identified between the SAL-mediated anti-hypoxia and $CoCl_2$-induced hypoxic group. The 165 DEPs were significantly enriched in processes related to cell cycle regulation, spindle checkpoint control, DNA repair, and response to ROS processes. On the other hand, the 266 DPSs were significantly enriched in actin filament-based processes, Rho GTPases signaling, response to epidermal growth factor, and apoptotic processes. Furthermore, combined with the results of quantitative proteomics and Western blot, we revealed that the expression levels of related molecules involved in regulating oxygen signaling or response to stress were obviously changed, including down-regulated expression of hypoxia-inducible factor 1 alpha subunit (HIF1A), heme oxygenase 1 (HMOX1), TNFα induced protein 2 (TNFAIP), sulfiredoxin 1 (SRXN1), and kelch like ECH associated protein 1 (Keap1), and up-regulated expression of reactive oxygen species modulator 1 (ROMO1). The HIF1A and HMOX1, as important molecules in response to hypoxia stress, play a pivotal role in maintaining normal energy metabolism, enhancing oxygen transport, and facilitating metabolic adaptation to hypoxia [40,41]. SRXN1 functions as an oxidative stress resistance factor that sustains intracellular Redox balance [42]. Keap1 act as an important sensor of oxidative stress and interacts with Nrf2 to regulate the cellular response to oxidative stress [43]. The activation of NFκB and TNF-mediated cell apoptosis may be promoted by TNFAIP [44], leading to a down-regulation in the expression level of TNFAIP induced by SAL, which subsequently inhibits $CoCl_2$-induced immune and inflammatory responses. Additionally, ROMO1 regulated mitochondrial cristae junction via enhancing OPA1 oligomerization to alleviate oxidative stress-related damage [45]. Therefore, we proposed that SAL could alleviate the $CoCl_2$-induced hypoxic effect by upregulating ROMO1 expression and downregulating HIF1A, HMOX1, SRXN1 and Keap1 expression in cell.

We also noticed that SAL upregulated the expression levels of proteins involved in DNA replication and repair processes against the $CoCl_2$-induced hypoxia effect, including chromatin assembly factor 1A (CHAF1A), CHAF1B, DNA heat shock protein family member C9 (DNAJC9), DNA methyltransferase 1 (DNMT1), DNA replication and sister chromatid cohesion 1 (DSCC1), DNA ligase 1 (LIG1), DNA polymerase alpha 1 (POLA1), DNA polymerase epsilon (POLE), DNA primase subunit 1(PRIM1), replication factor C1 (RFC1), RFC3, RFC5 and DNA topoisomerase II alpha (TOP2A). We also found that SAL upregulated the expression levels of related structural proteins to microtubules and centromere, such as 8 KIF members and inner centromere protein (INCENP). Meanwhile, 5 microtubule-associated proteins (MAPs) contained fifteen phosphosites in SAL-mediated anti-hypoxia group were significantly reduced abundance than those of $CoCl_2$-induced hypoxia group, including MAP1A (750T, 2150S, 2443S, 2459S), MAP1B (1254S, 1321S, 1797S), MAP2 (46S, 1795S, 1799S, 1801S, 1807S, 1810S), MAP4 (627S) and MAP6 (685S). The process of microtubule assembly consisted of α and β heterodimers, polymerized to form polar fibrils and formed the microtubules. This assembly-dissociation process is accompanied by

dynamic tubulin dephosphorylation and phosphorylation transformations [46]. Otherwise, SAL could antagonize $CoCl_2$-mediated G_2/M cell cycle arrest. Compared to the $CoCl_2$ treatment group, the expression levels of AURKA, AURKB, marker of proliferation Ki-67 (MKI67), polo-like kinase 1(PLK1), CDKN2A, timeless circadian regulator (TIMELESS), cell division cycle associated 5(CDCA5), CCND3 and p-C-Jun(70S,76S) were significantly uupregulated. AURKA and AURKB belonged to cell cycle-regulating kinases that formed and stabilized the spindle polar microtubules during chromosome separation [47]. CDCA5 located in the nucleoplasm was involved in DNA double-strand break repair and regulated the cell cycle process [48]. MKI67 is a nuclear protein essential for cell proliferation while PLK1 is a serine/threonine-protein kinase crucial for this process [49,50]. TIMELESS primarily ensures cellular survival during injury or stress by enhancing POLE activity and maintaining telomere length as well as regulating cell morphogenesis [51]. C-Jun and C-Fos in the nucleus were phosphorylated by ERK signal followed by activated to form the transcriptional regulatory complex AP1, which could promote cell proliferation [52]. Additionally, our study observed a significant increase in mTOR expression level under $CoCl_2$-induced hypoxia compared to control group which was subsequently reduced upon SAL treatment. We hypothesize that activation of mTOR might induce cardiomyocyte senescence.

5. Conclusions

In summary, in this study, we applied the integrative proteomics and phosphoproteomics to study the molecular alteration landscape at both protein and phosphoprotein levels of salidroside in ameliorating myocardial hypoxia. In particularly, we firstly constructed the phosphorylation landscape of salidroside treatment. Combine with the validation by using western-blot and Mn^{2+}-phos-tag page gels analysis, confirmed that SAL had the ability to protect myocardial cells against $CoCl_2$-induced hypoxia through multiple biological pathways, including enhancing the spindle stability, maintaining the cell cycle, relieving the DNA damage, and antagonizing cell apoptosis.

This study provides an in-depth analytical dataset of proteome and phosphorylated proteome for anti-hypoxic research of SAL, offering a systematic perspective on the alterations at protein and protein phosphorylation levels induced by SAL treatment, thereby enhancing our understanding of its underlying mechanism. Furthermore, our study provides a valuable resource for further investigating the effects of SAL. However, there are some limitations in our study. Firstly, this study focused solely on cellular-level investigations without animal models. Secondly, this study didn't conduct the SAL-direct target screen analysis. In the future studies, we aim to establish the animal model to explore the precise anti-hypoxic mechanism mediated by SAL. Additionally, we will design chemical probes based on the structure of SAL and employ ABPP technology for screening SAL direct targets [53] *(Chem Soc Rev. 2011 Jan;40(1):246-57.)*.

CRediT authorship contribution statement

Zhongwei Xu: Writing – review & editing, Writing – original draft, Methodology, Formal analysis. **Kaiyuan Fan:** Writing – review & editing, Writing – original draft, Methodology, Formal analysis. **Heng Li:** Writing – original draft, Methodology, Formal analysis, Data curation. **Lulu Wang:** Writing – review & editing, Writing – original draft, Methodology, Formal analysis. **Wenqing Zhu:** Methodology. **Shuang Zou:** Methodology. **Yan Zhang:** Data curation. **Yanan Liu:** Formal analysis. **Zhidong Wu:** Formal analysis. **Qian Gong:** Methodology. **Minjia Tan:** Writing – review & editing. **Jin Wang:** Writing – review & editing, Writing – original draft, Visualization, Supervision, Investigation, Conceptualization, Jia Guo, Methodology. **Linhui Zhai:** Writing – review & editing, Writing – original draft, Supervision, Project administration, Methodology, Investigation, Formal analysis, Conceptualization.

Declaration of competing interest

The authors declare that they have no known competing financial interests or personal relationships that could have appeared to influence the work reported in this paper.

Acknowledgements

This study was supported by grants from the National Natural Science Foundation of China (No.32171434), the PLA Medical Science and technology youth training program (No.18QNP044), the China People's Armed Regular Forces Personnel Project Plan (ZZKY20222308), the Science and Technology Commission of Qingpu District, Shanghai (QKY2021-02), the Doctoral Fund of Qingpu Branch of Zhongshan Hospital Affiliated to Fudan University (IDQYBS2022-02).

Appendix A. Supplementary data

Supplementary data to this article can be found online at https://doi.org/10.1016/j.heliyon.2024.e30433.

References

[1] H.A. Prag, D. Aksentijevic, A. Dannhorn, A.V. Giles, J.F. Mulvey, O. Sauchanka, L. Du, G. Bates, J. Reinhold, D. Kula-Alwar, Ischemia-selective cardioprotection by malonate for ischemia/reperfusion injury, Circ. Res. 131 (6) (2022) 528–541, https://doi.org/10.1161/CIRCRESAHA.121.320717.

[2] B. Luo, Y. Li, M. Zhu, J. Cui, Y. Liu, Y. Liu, Intermittent hypoxia and atherosclerosis: from molecular mechanisms to the therapeutic treatment, Oxid. Med. Cell. Longev. 2022 (2022), https://doi.org/10.1155/2022/1438470.

[3] X. Wang, H. Sun, L. Cui, X. Wang, C. Ren, Z. Tong, X. Ji, Acute high-altitude hypoxia exposure causes neurological deficits via formaldehyde accumulation, CNS Neurosci. Ther. 28 (8) (2022) 1183–1194, https://doi.org/10.1111/cns.13849.

[4] P. Murugesan, Y. Zhang, J.Y. Youn, H. Cai, Novel and robust treatment of pulmonary hypertension with netrin-1 and netrin-1-derived small peptides, Redox Biol. 55 (2022) 102348, https://doi.org/10.1016/j.redox.2022.102348.

[5] S. Leroux, A. Rodriguez-Duboc, A. Arabo, M. Basille-Dugay, D. Vaudry, D. Burel, Bioscience, Intermittent hypoxia in a mouse model of apnea of prematurity leads to a retardation of cerebellar development and long-term functional deficits, Cell Biosci. 12 (1) (2022) 148, https://doi.org/10.1186/s13578-022-00869-5.

[6] R. Alcantud, J. Weiss, M.I. Terry, N. Bernabé, F. Verdú-Navarro, J.T. Fernández-Breis, M. Egea-Cortines, Flower transcriptional response to long term hot and cold environments in Antirrhinum majus, Front. Plant Sci. 14 (2023) 1120183, https://doi.org/10.3389/fpls.2023.1120183.

[7] R. He, R. Ma, Z. Jin, Y. Zhu, F. Yang, F. Hu, J. Dai, Proteomics and metabolomics unveil codonopsis pilosula (franch.) nannf. Ameliorates gastric precancerous lesions via regulating energy metabolism, Front. Pharmacol. 13 (2022) 933096, https://doi.org/10.3389/fphar.2022.933096.

[8] K. Hu, T.M. Yan, K.Y. Cao, F. Li, X.R. Ma, Q. Lai, J.C. Liu, Y. Pan, J.P. Kou, Z.H. Jiang, A tRNA-derived fragment of ginseng protects heart against ischemia/reperfusion injury via targeting the lncRNA MIAT/VEGFA pathway, Mol. Ther. Nucleic Acids 29 (2022) 672–688, https://doi.org/10.1016/j.omtn.2022.08.014.

[9] N. Xie, F. Fan, S. Jiang, Y. Hou, Y. Zhang, N. Cairang, X. Wang, X. Meng, Rhodiola crenulate alleviates hypobaric hypoxia-induced brain injury via adjusting NF-κB/NLRP3-mediated inflammation, Phytomedicine 103 (2022) 154240, https://doi.org/10.1016/j.phymed.2022.154240.

[10] T.T. Le, S.R. McGrath, P.S. Fasinu, Herb-drug interactions in Neuropsychiatric Pharmacotherapy–A review of clinically Relevant findings, Curr. Neuropharmacol. 20 (9) (2022) 1736, https://doi.org/10.2174/1570159X19666210809100357.

[11] J. Han, L. Luo, Y. Wang, S. Wu, V. Kasim, Therapeutic potential and molecular mechanisms of salidroside in ischemic diseases, Front. Pharmacol. 13 (2022) 974775, https://doi.org/10.3389/fphar.2022.974775.

[12] Q. Guo, J. Yang, Y. Chen, X. Jin, Z. Li, X. Wen, Q. Xia, Y. Wang, Salidroside improves angiogenesis-osteogenesis coupling by regulating the HIF-1α/VEGF signalling pathway in the bone environment, Eur. J. Pharmacol. 884 (2020) 173394, https://doi.org/10.1016/j.ejphar.2020.173394.

[13] H.B. Li, Y.k. Ge, X.X. Zheng, L. Zhang, Salidroside stimulated glucose uptake in skeletal muscle cells by activating AMP-activated protein kinase, Eur. J. Pharmacol. 588 (2–3) (2008) 165–169, https://doi.org/10.1016/j.ejphar.2008.04.036.

[14] L. Zhu, T. Wei, J. Gao, X. Chang, H. He, F. Luo, R. Zhou, C. Ma, Y. Liu, T. Yan, The cardioprotective effect of salidroside against myocardial ischemia reperfusion injury in rats by inhibiting apoptosis and inflammation, Apoptosis 20 (2015) 1433–1443, https://doi.org/10.1007/s10495-015-1174-5.

[15] D. Zhao, X. Sun, S. Lv, M. Sun, H. Guo, Y. Zhai, Z. Wang, P. Dai, L. Zheng, M. Ye, Salidroside attenuates oxidized low-density lipoprotein-induced endothelial cell injury via promotion of the AMPK/SIRT1 pathway, Int. J. Mol. Med. 43 (6) (2019) 2279–2290, https://doi.org/10.3892/ijmm.2019.4153.

[16] L. Tu, C. Li, X. Xiong, J. Hyeon Kim, Q. Li, L. Mei, J. Li, S. Liu, J. Seung Kim, Y. Sun, Engineered metallacycle-based supramolecular Photosensitizers for effective Photodynamic Therapy, Angew. Chem. 135 (15) (2023) e202301560, https://doi.org/10.1002/ange.202301560.

[17] C. Li, Y. Pang, Y. Xu, M. Lu, L. Tu, Q. Li, A. Sharma, Z. Guo, X. Li, Y. Sun, Near-infrared metal agents assisting precision medicine: from strategic design to bioimaging and therapeutic applications, Chem. Soc. Rev. (2023), https://doi.org/10.1039/D3CS00227F.

[18] Y. Xu, C. Li, X. Ma, W. Tuo, L. Tu, X. Li, Y. Sun, P.J. Stang, Y. Sun, Long wavelength–emissive Ru (II) metallacycle–based photosensitizer assisting in vivo bacterial diagnosis and antibacterial treatment, Proc. Natl. Acad. Sci. U.S.A. 119 (32) (2022) e2209904119, https://doi.org/10.1073/pnas.2209904119.

[19] L. Chen, P. Liu, X. Feng, C. Ma, Salidroside suppressing LPS-induced myocardial injury by inhibiting ROS-mediated PI 3K/Akt/mTOR pathway in vitro and in vivo, J. Cell Mol. Med. 21 (12) (2017) 3178–3189, https://doi.org/10.1111/jcmm.12871.

[20] L.h. Zhai, K.f. Chen, B.b. Hao, M.j. Tan, Proteomic characterization of post-translational modifications in drug discovery, Acta Pharmacol. Sin. 43 (12) (2022) 3112–3129, https://doi.org/10.1038/s41401-022-01017-y.

[21] L. Chen, X. Zhang, Q. Zhang, T. Zhang, J. Xie, W. Wei, Y. Wang, H. Yu, H. Zhou, A necroptosis related prognostic model of pancreatic cancer based on single cell sequencing analysis and transcriptome analysis, Front. Immunol. 13 (2022) 1022420, https://doi.org/10.3389/fimmu.2022.1022420.

[22] H. Sies, Oxidative stress: a concept in redox biology and medicine, Redox Biol. 4 (2015) 180–183, https://doi.org/10.1016/j.redox.2015.01.002.

[23] Z. Xu, X. Jin, W. Cai, M. Zhou, P. Shao, Z. Yang, R. Fu, J. Cao, Y. Liu, F. Yu, Proteomics analysis reveals abnormal electron transport and excessive oxidative stress cause mitochondrial dysfunction in placental tissues of early-onset preeclampsia, Proteonomics Clin. Appl. 12 (5) (2018) 1700165, https://doi.org/10.1002/prca.201700165.

[24] S.J. Humphrey, O. Karayel, D.E. James, M. Mann, High-throughput and high-sensitivity phosphoproteomics with the EasyPhos platform, Nat. Protoc. 13 (9) (2018) 1897–1916, https://doi.org/10.1038/s41596-018-0014-9.

[25] B. Li, F. Guo, H. Hu, P. Liu, M. Tan, J. Pan, L. Zhai, The characterization of column heating effect in nanoflow liquid chromatography mass spectrometry (nanoLC-MS)–based proteomics, J. Mass Spectrom. 55 (1) (2020) e4441, https://doi.org/10.1002/jms.4441.

[26] J.J. Liu, K. Sharma, L. Zangrandi, C. Chen, S.J. Humphrey, Y.-T. Chiu, M. Spetea, L.-Y. Liu-Chen, C. Schwarzer, M. Mann, In vivo brain GPCR signaling elucidated by phosphoproteomics, Science 360 (6395) (2018) eaao4927, https://doi.org/10.1126/science.aao4927.

[27] G.O. Consortium, Gene ontology consortium: going forward, Nucleic Acids Res. 43 (D1) (2015) D1049–D1056, https://doi.org/10.1093/nar/gku1179.

[28] Y. Zhou, B. Zhou, L. Pache, M. Chang, A.H. Khodabakhshi, O. Tanaseichuk, C. Benner, S.K. Chanda, Metascape provides a biologist-oriented resource for the analysis of systems-level datasets, Nat. Commun. 10 (1) (2019) 1523, https://doi.org/10.1038/s41467-019-09234-6.

[29] Y. Kwon, S. Lee, N. Park, S. Ju, S. Shin, S. Yoo, H. Lee, C. Lee, Phosphoproteome profiling using an isobaric carrier without the need for phosphoenrichment, Anal. Chem. 94 (10) (2022) 4192–4200, https://doi.org/10.1021/acs.analchem.1c04188.

[30] E. Kinoshita-Kikuta, E. Kinoshita, A. Matsuda, T. Koike, Tips on improving the efficiency of electrotransfer of target proteins from Phos-tag SDS-PAGE gel, Proteomics 14 (21–22) (2014) 2437–2442, https://doi.org/10.1002/pmic.201400380.

[31] Y. Lu, B. Deng, L. Xu, H. Liu, Y. Song, F. Lin, Effects of Rhodiola Rosea supplementation on exercise and sport: a systematic review, Front. Nutr. 9 (2022) 856287, https://doi.org/10.3389/fnut.2022.856287.

[32] Z. Pang, N. Ran, Y. Yuan, C. Wang, G. Wang, H. Lin, A.C.-Y. Hsu, J. Liu, F. Wang, Phenotype-specific therapeutic effect of Rhodiola wallichiana var. cholaensis combined with dexamethasone on experimental murine asthma and its comprehensive pharmacological mechanism, Int J Mol Cell Med 20 (17) (2019) 4216, https://doi.org/10.3390/ijms20174216.

[33] X. Ding, Z. Zhang, J. Jin, J. Han, Y. Wang, K. Yang, Y. Yang, H. Wang, X. Dai, C. Yao, Salidroside can target both P4HB-mediated inflammation and melanogenesis of the skin, Theranostics 10 (24) (2020) 11110, https://doi.org/10.7150/thno.47413.

[34] Y. Li, Y. Cao, J. Xiao, J. Shang, Q. Tan, F. Ping, W. Huang, F. Wu, H. Zhang, X. Zhang, Inhibitor of apoptosis-stimulating protein of p53 inhibits ferroptosis and alleviates intestinal ischemia/reperfusion-induced acute lung injury, Cell Death Differ. 27 (9) (2020) 2635–2650, https://doi.org/10.1038/s41418-020-0528-x.

[35] N. Xing, J. Qin, D. Ren, Q. Du, Y. Li, J. Mi, F. Zhang, L. Ai, S. Zhang, Y. Zhang, Integrating UPLC-Q-Exactive Orbitrap/MS, network pharmacology and experimental validation to reveal the potential mechanism of Tibetan medicine Rhodiola granules in improving myocardial ischemia-reperfusion injury, J. Ethnopharmacol. 314 (2023) 116572, https://doi.org/10.1016/j.jep.2023.116572.

[36] F. Chen, Y. Chai, F. Zhang, Y. Liu, Y. Zhang, Y. Shi, J. Zhang, Y. Leng, Network pharmacology analysis combined with experimental validation to explore the therapeutic mechanism of salidroside on intestine ischemia reperfusion, Biosci. Rep. 43 (8) (2023), https://doi.org/10.1042/BSR20230539.

[37] Z. Zhang, L. Wu, T. Cui, R.Z. Ahmed, H. Yu, R. Zhang, Y. Wei, D. Li, Y. Zheng, W. Chen, Oxygen sensors mediated HIF-1α accumulation and translocation: a pivotal mechanism of fine particles-exacerbated myocardial hypoxia injury, Environ. Pollut. 300 (2022) 118937, https://doi.org/10.1016/j.envpol.2022.118937.

[38] Z. Huang, W. Xu, J. Wu, X. Lu, X. Chen, MicroRNA-374a protects against myocardial ischemia-reperfusion injury in mice by targeting the MAPK6 pathway, Life Sci. 232 (2019) 116619, https://doi.org/10.1016/j.lfs.2019.116619.
[39] N.K. Rana, P. Singh, B. Koch, CoCl 2 simulated hypoxia induce cell proliferation and alter the expression pattern of hypoxia associated genes involved in angiogenesis and apoptosis, Biol. Res. 52 (12) (2019) 1–13, https://doi.org/10.1186/s40659-019-0221-z.
[40] R. Liu, C. Xu, W. Zhang, Y. Cao, J. Ye, B. Li, S. Jia, L. Weng, Y. Liu, L. Liu, FUNDC1-mediated mitophagy and HIF1α activation drives pulmonary hypertension during hypoxia, Cell Death Dis. 13 (7) (2022) 634, https://doi.org/10.1038/s41419-022-05091-2.
[41] J. Shi, T. Yu, K. Song, S. Du, S. He, X. Hu, X. Li, H. Li, S. Dong, Y. Zhang, Dexmedetomidine ameliorates endotoxin-induced acute lung injury in vivo and in vitro by preserving mitochondrial dynamic equilibrium through the HIF-1a/HO-1 signaling pathway, Redox Biol. 41 (2021) 101954, https://doi.org/10.1016/j.redox.2021.101954.
[42] J. He, M. Ma, D. Li, K. Wang, Q. Wang, Q. Li, H. He, Y. Zhou, Q. Li, X. Hou, disease, Sulfiredoxin-1 attenuates injury and inflammation in acute pancreatitis through the ROS/ER stress/Cathepsin B axis, Cell Death Dis. 12 (7) (2021) 626, https://doi.org/10.1038/s41419-021-03923-1.
[43] Z. Tang, B. Hu, F. Zang, J. Wang, X. Zhang, H. Chen, Nrf2 drives oxidative stress-induced autophagy in nucleus pulposus cells via a Keap1/Nrf2/p62 feedback loop to protect intervertebral disc from degeneration, Cell Death Dis. 10 (7) (2019) 510, https://doi.org/10.1038/s41419-019-1701-3.
[44] I. Matsumoto, A. Inoue, C. Takai, N. Umeda, Y. Tanaka, Y. Kurashima, T. Sumida, Regulatory roles of tumor necrosis factor alpha-induced proteins (TNFAIPs) 3 and 9 in arthritis, Clin. Immunol. 153 (1) (2014) 73–78, https://doi.org/10.1016/j.clim.2014.03.015.
[45] G.Y. Lee, D.g. You, H.R. Lee, S.W. Hwang, C.J. Lee, Y.D. Yoo, Romo1 is a mitochondrial nonselective cation channel with viroporin-like characteristics, J. Cell Biol. 217 (6) (2018) 2059–2071, https://doi.org/10.1083/jcb.201709001.
[46] P. Binarová, J.J.C. Tuszynski, Tubulin: structure, functions and roles in disease, Cells 8 (10) (2019) 1294, https://doi.org/10.3390/cells8101294.
[47] H.T. Huang, D. Dobrovolsky, J. Paulk, G. Yang, E.L. Weisberg, Z.M. Doctor, D.L. Buckley, J.-H. Cho, E. Ko, J. Jang, A chemoproteomic approach to query the degradable kinome using a multi-kinase degrader, Cell Chem. Biol. 25 (1) (2018) 88–99. e6, https://doi.org/10.1016/j.chembiol.2017.10.005.
[48] C. Gelot, J. Guirouilh-Barbat, T. Le Guen, E. Dardillac, C. Chailleux, Y. Canitrot, B.S. Lopez, The cohesin complex prevents the end-joining of distant DNA double-strand ends in S phase: Consequences on genome stability maintenance, Nucleus 7 (4) (2016) 339–345, https://doi.org/10.1080/19491034.2016.1194159.
[49] T. Kim, Recent progress on the localization of PLK1 to the Kinetochore and its role in Mitosis, Int. J. Mol. Sci. 23 (9) (2022) 5252, https://doi.org/10.3390/ijms23095252.
[50] S. Uxa, P. Castillo-Binder, R. Kohler, K. Stangner, G.A. Müller, K. Engeland, Ki-67 gene expression, Cell Death Differ. 28 (12) (2021) 3357–3370, https://doi.org/10.1038/s41418-021-00823-x.
[51] J.A. Patel, H. Kim, The TIMELESS effort for timely DNA replication and protection, Cell. Mol. Life Sci. 80 (4) (2023) 84, https://doi.org/10.1007/s00018-023-04738-3.
[52] T. Miyake, J.C. McDermott, Nucleolar localization of c-Jun, FEBS J. 289 (3) (2022) 748–765, https://doi.org/10.1111/febs.16187.
[53] W.P. Heal, T.T. Dang, E.W. Tate, Activity-based probes: discovering new biology and new drug targets, Chem. Soc. Rev. 40 (1) (2011) 246–257, https://doi.org/10.1039/C0CS00004C.